Available online at www.sciencedirect.com

ScienceDirect

Ceramics International 41 (2015) 8425–8432

CERAMICS INTERNATIONAL

www.elsevier.com/locate/ceramint

Mechanical properties of porous ceramic scaffolds: Influence of internal dimensions

I. Sabree, J.E. Gough, B. Derby*

School of Materials, University of Manchester, Oxford Road, Manchester M13 7PL, UK

Received 20 February 2015; received in revised form 6 March 2015; accepted 9 March 2015
Available online 17 March 2015

Abstract

Highly porous ceramic scaffolds have been fabricated from a 70% SiO_2–30% CaO glass powder using stereolithography and the lost-mould process combined with gel-casting. After sintering at 1200 °C the glass crystallised to a structure of wollastonite and pseudowollastonite grains in a glassy matrix with a bulk porosity of 1.3%. All scaffolds had a simple cubic strut structure with an internal porosity of approximately 42% and internal pore dimensions in the range 300–600 μm. The mean crushing strength of the scaffolds is in the range 10–25 MPa with the largest pore sizes showing the weakest strengths. The variability of scaffold strengths has been characterised using Weibull statistics and each set of scaffolds showed a Weibull modulus of $m \approx 3$ independent of pore size. The equivalent strength of the struts within the porous ceramics was estimated to be in the range 40–80 MPa using the models of the Gibson and Ashby. These strengths were found to scale with specimen size consistent with the Weibull modulus obtained from compression tests. Using a Weibull analysis, these strengths are shown to be in accordance with the strength of 3-point bend specimens of the bulk glass material fabricated using identical methods. The strength and Weibull modulus of these scaffolds are comparable to those reported for other porous ceramic scaffold materials of similar porosity made by different fabrication routes.

Keywords: Porous ceramics; Stereolithography; Gel casting; Weibull statistics

1. Introduction

The scaffold is a key concept in tissue engineering. This is a porous structure that acts as a substrate, upon the surface of which cells adhere and grow. The scaffold provides structural and mechanical support as well as the surface for cell growth. Its presence allows cells to generate the biological structural components of the extracellular matrix (ECM) in culture conditions. After a suitable period of culture and after implantation into a host, sufficient ECM will produce an appropriate tissue to provide mechanical integrity and the scaffold will either be harmlessly incorporated or degrade, dissolve and ultimately be excreted. For many applications, especially in the area of bone tissue engineering, this scaffold will be fabricated from an inorganic ceramic or glass [1]. The material composition of the scaffold, its gross architecture (dimensions of its walls, pores and channels), the material microstructure and crystallinity all play a part in controlling the local environment and well being of the cells located within it [2–4].

The appropriate architecture and dimensions of a suitable scaffold are determined by a number of requirements for biocompatibility. An important role of the scaffold is to provide a temporary home for the growth and culture of cells in a bioreactor environment. Within a living tissue, cells are maintained in good health by a supply of oxygen and nutrients and the removal of carbon dioxide and waste through the capillary network. Each cell must be sufficiently close to the network to allow diffusional transport within an appropriate time scale. By analogy, all cells within the scaffold must have a similar access requirement, and this is normally achieved by providing a structure with a high level of porosity of an appropriate dimension to allow the uninterrupted flow of fluid within a bioreactor. Hutmacher has reviewed the architectural and topological requirements of scaffold design for tissue engineering cell culture [2].

*Corresponding author.

http://dx.doi.org/10.1016/j.ceramint.2015.03.044

Highly porous scaffold designs possess a large surface area, which favours cell attachment and growth. Porosity, ranging from 40% to 90% in a variety of materials, encourages osteointegration with the implant surface and promotes adhesion of the implant [5]. In addition, a porous surface enhances a mechanical interlock between the scaffold and host tissue [6]. The mean pore size of a scaffold controls cell adhesion, migration, tissue formation, nutrient and oxygen access as well as waste removal [7]. Hulbert defined a minimum pore size for a scaffold at 100 μm [8]. However, later studies have shown that better osteogenesis occurs with a pore size >300 μm [5,6]. In addition, the pores should be interconnected. The interconnection size will be smaller than the pore size but if must be sufficient to permit cell migration, communication between cells and ECM formation between the pores. It is well known that the porosity of a foamed structure has lower mechanical properties (elastic constants, ultimate strength, fracture resistance) than the equivalent bulk material and that these reduced properties are a function of the relative density (1 – porosity) of the foam [9]. Thus, when using porous structures for tissue engineering scaffolds, the structure must retain sufficient mechanical properties to fulfil the requirements of structural integrity once implanted in host tissue. For bone tissue engineering applications the consensus is that ceramic and inorganic materials should have mechanical properties similar to that of bone. However, the mechanical properties of bone have a large range of reported values and depend on the local density of the tissue and testing environment. For example, cortical bone has a reported Young's modulus in the range 1–20 GPa and a strength range of 1–100 MPa [10], with the equivalent values for cancellous (trabecular) bone of Young's modulus 0.1–1.0 GPa and strength 1–10 MPa [11]. Despite the large range in the reported mechanical properties of bone, these act as a guide to the required mechanical properties of a scaffold.

There have been a number of different microstructures or architectures of highly porous ceramic and glass scaffolds that have been used for tissue engineering applications. These can be broadly divided into two classes: random porosity and designed porosity. Random pore architectures display a structure showing no significant long range order or alignment to the pore distribution, with pore size and shape showing significant variation around the mean values. Such structures are generally termed ceramic foams and they can be achieved by methods such as casting a slurry around a sacrificial polymer foam template, using poro-generators such as a soluble salt or polymer microbeads and by the addition of surfactant foaming agents and stabilisers prior to gaseous foaming [1,12–15]. Although it is possible to control some aspects of the foam structure (mean cell size and wall thickness), they are random on a local scale and any microstructural control is of the average properties of the structure. A second set of manufacturing processes must be used in order to achieve a more precise control of porous ceramic scaffolds and define both pore and interconnection size. These are variously described as rapid prototyping, additive manufacture or 3D printing. These manufacturing technologies fabricate structures with a spatial resolution or feature size >30 μm and can be used to explicitly define and fabricate a bespoke structure [16,17].

The basic requirements of a scaffold material are high cell/tissue biocompatibility, non-toxicity, capability of promoting cell proliferation and differentiation, and sufficient mechanical properties. Bioactive glasses have remarkable advantages such as good biocompatibility, osteoproductivity and osteoconductivity [18]. Various studies have determined that ionic dissolution products from bioactive glasses can enhance osteogenesis by activating genes found in osteoblasts and stimulating regeneration of bone tissue [19–21]. In this study we have selected a phosphate-free bioactive glass of composition 70% SiO_2–30% CaO. This composition is known to support osteoblast growth and induce differentiation when used to form scaffold materials [22]. We have chosen the process of indirect manufacture to form scaffold structures based on the 70% SiO_2–30% CaO glass composition. This uses the additive manufacture route of stereolithography to fabricate moulds that define the scaffold internal architecture and feature dimensions. These moulds are used to manufacture the scaffolds using the gel-casting process following the general procedures originally pioneered by Halloran and co-workers [23]. A range of scaffolds have been manufactured with different pore sizes but the same overall porosity to explore how the pore size influences scaffold strength.

2. Methods

2.1. Scaffold materials and fabrication

Phosphate-free bioactive glass powder, of composition 70% SiO_2–30% CaO_2, was provided by Julian Jones and Gowishan Poologasundarampillai (Imperial College, London, UK). This had an as-received mean particle size of approximately 50 μm, which was reduced to a size suitable for processing and sintering by milling. Glass powder (150 g) was mixed with 250 ml distilled water and two to three drops of Dolapix CE64 added (Zschimmer & Schwarz, Lahnstein, Germany) before processing in an attrition mill using ZrO_2 milling media (Szegvari Attritor System, Union Process, Akron, OH, USA). At the end of the milling process the slurry was separated from the milling media and freeze dried (Micro Modulyo, Edwards, Hastings, UK). The freeze dried powder had a mean particle size of 3.2 μm measured by light scattering (Mastersizer Plus, Malvern Instruments, Great Malvern, UK).

To manufacture the scaffolds we used a modification of the "lost-mould" process for ceramic manufacture. Here a polymer mould is used to define the complex shape of a ceramic (or glass) body prior to high temperature sintering. The mould is filled with fine particles of the ceramic or glass in suspension in a fluid of cross-linkable oligomers. The fluid is gelled by an external stimulus, usually mild heating to form a composite block of the mould and the ceramic in a polymer matrix (gel casting). The polymers are removed by a heat treatment in air as part of the thermal cycle during sintering. Gel casting and

the choice of suitable oligomers have been reviewed by Janney et al. [24,25].

The gel casting suspension used in this study was based on prior published work of Chu [23] and Chopra [26]; it comprised two low viscosity monomers: Isobornyl acrylate (IBA) and Propoxylated neopentoglycol diacrylate (PNPGDA) both sourced from Sigma-Aldrich (Gillingham, UK), mixed 1:1 by weight. The suspension was produced by mixing the monomers with 5 wt% of glass powder and Variquat CC42 NS (Evonik, Essen, Germany) as a surfactant in order to generate good homogeneity and a low suspension viscosity. The slurry was then mixed with (1.4–1.7) mm diameter zirconia balls in a polyethylene container and placed in a high speed mixer at 1500 rpm for 10 min. The bioactive glass powder was added gradually with 10 min of mixing for each step. The final slurry contains approximately 50% by volume glass powder and has a viscosity of approximately 2 Pa s. After homogenisation, 1 wt% of Benzoyl Peroxide (BPO) (Sigma-Aldrich) was added to the suspension as a thermal initiator for the polymerisation of the resin. Immediately prior to casting the resin was degassed in a vacuum chamber at 7×10^{-2} mbar for 1 h.

Moulds were fabricated by stereolithography (SLA) using a Viper Si2TM SLA system (3D Systems Inc., Rock Hill, SC, USA) using a proprietary epoxy based resin system, Accura Amethyst (3D Systems). The study used three scaffold designs; all of these had a simple cubic lattice with dimensions scaled so that after shrinkage during sintering the resulting scaffolds had pore sizes of 300 μm, 400 μm and 600 μm with a porosity of approximately 42% measured after processing. These 3D scaffolds will be referred as 300scaf, 400scaf, and 600scaf respectively. Following gel-casting, the mould and slurry were placed in a vacuum chamber for further degassing and then heated at 80 °C for 30 min to promote cross-linking and gelation/solidification of the suspension. To fabricate the final bioactive glass scaffolds it was necessary to hold the gelcast suspension and mould at 550 °C for 2 h in air, in order to burn out the epoxy mould and the acrylic monomers. After this the sample temperature was raised to a temperature in the range 800–1200 °C prior to sintering. Fig. 1 shows examples of the moulds and subsequent fabricated scaffolds. In order to characterise the bulk properties of the scaffold materials, dense bars of dimensions $3.5 \pm 0.4 \times 4.5 \pm 0.4 \times 30$ mm were used. These bars were cut from larger plates produced from the ceramic suspension using identical gel-cast fabrication methods as with the scaffolds.

2.2. Scaffold characterisation

Specimens of the sintered scaffolds were characterised by X-ray diffraction (XRD) (Philips Analytical X-ray, Bi-Sonic Technology Corp., Model: 3C-230HB, Philips, Eindhoven, Netherlands) to identify crystal phases present. The scaffold internal architecture and microstructure were examined by scanning electron microscopy (SEM) (JSM 6300, JEOL, Tokyo, Japan). Samples were coated with gold for 4 min (Sputter Coater S150, Edwards, Hastings, UK) to prevent specimen charging. The elemental composition of the scaffolds

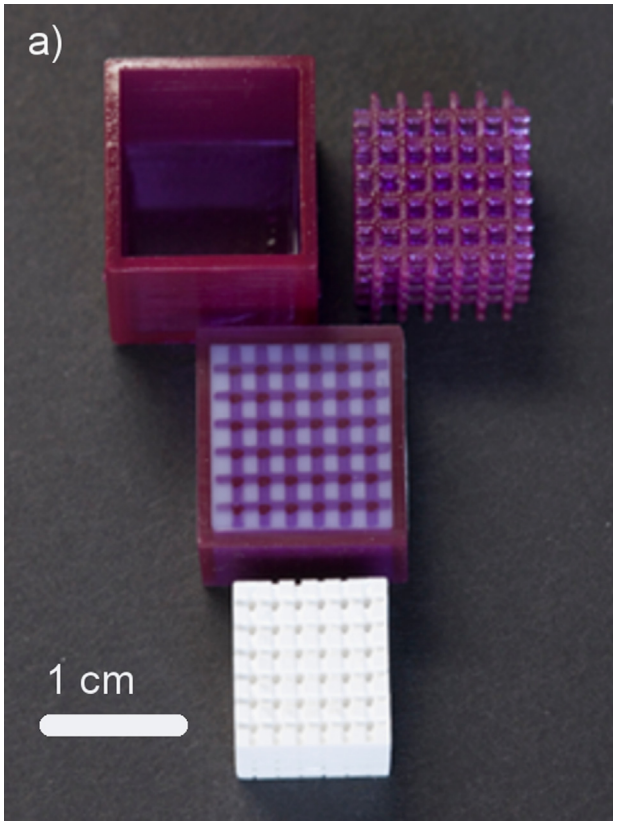

Fig. 1. Original mould fabricated by stereolithography, filled mould and final sintered 400scaf scaffold structure showing shrinkage after sintering.

was determined using an energy-dispersive X-ray (EDX) analysis which is an integrated feature of the SEM. For EDX analysis, samples were coated with carbon to avoid the overlap of one peak of gold with the k-line of phosphorus.

Scaffolds were tested in compression using a screw-driven load frame with 10 kN load capacity (5569H1549, Instron, High Wycombe, UK) at a constant crosshead velocity of 0.5 mm/min until crushing failure occurred. The compressive load and displacement were recorded at 0.1 s intervals during testing. Fifteen samples were tested for each type of scaffold in order to determine mean scaffold compressive strength, Young's modulus and Weibull modulus. Large test bars of dimensions 3.5 mm × 4.5 mm × 30 mm were tested in 4-point bend with an outer loaded length of 20 mm and inner length 10 mm. The mean modulus of rupture and Weibull modulus were calculated for these specimens. Nanoindentation was carried out using a NanoIndenter XP (Agilent, Santa Clara, CA, USA) to determine the hardness and elastic modulus of a cast bioactive glass disk which was sintered at 1200 °C. The specimens were embedded in an epoxy resin and polished in order to produce a good surface finish required for nanoindentation. Nanoindentation was carried out at a constant strain rate of 0.05 s^{-1}. In order to determine Young's modulus from unloading curves, Poisson's ratio was assumed to be 0.18 [27]. Two different samples were tested with 20 indentation different locations used in each to determine the average hardness and Young's modulus. Nanoindentation experiments

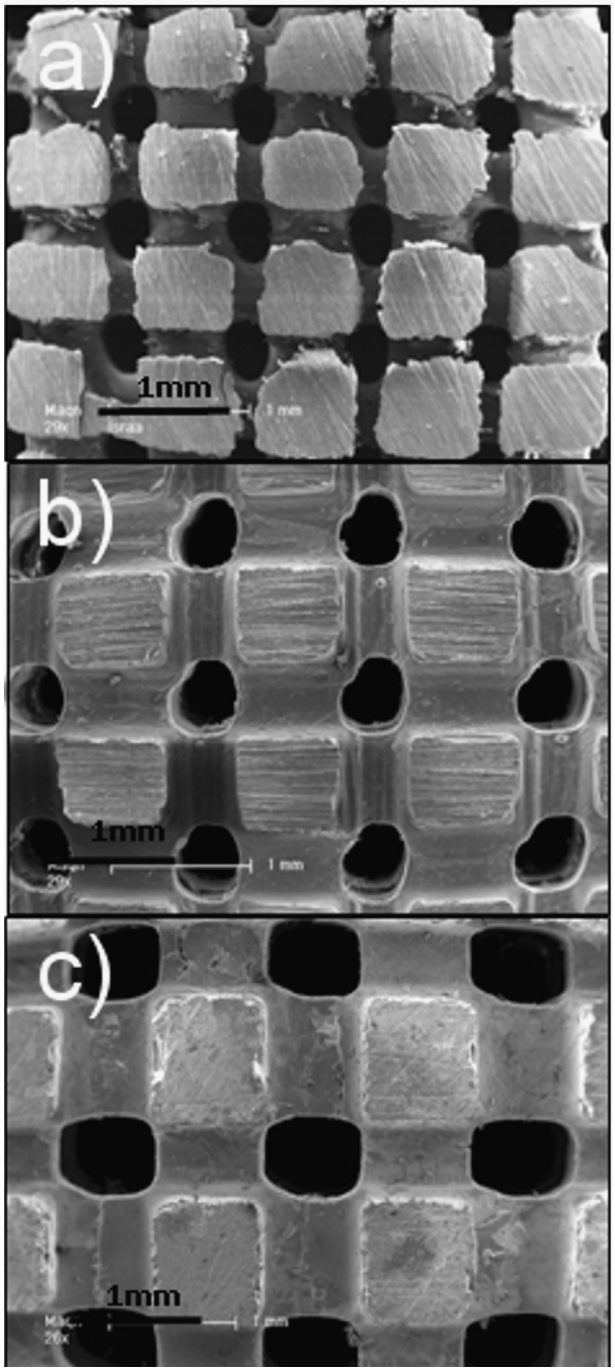

Fig. 2. SEM images showing a general view of the scaffolds' structure and morphology. All scaffolds have been sintered at 1200 °C. (a) 300scaf, (b) 400scaf, and (c) 600scaf.

were carried out following the procedure laid out in ISO 14577 for instrumented indentation.

3. Results and discussion

3.1. Scaffold architecture and microstructure

The architecture and internal structure of the three scaffolds after sintering at 1200 °C are shown in Fig. 2. There has been significant rounding of the original aquare section struts and channels during the sintering process but the final pore diameter is close to the designed value in each scaffold. Higher magnification images of struts after sintering at 800 and 1200 °C are shown in Fig. 3. It is clearly seen that at the lower temperature sintering is incomplete and the strut is highly porous. At 1200 °C the sintered structure shows a much higher degree of densification. However, as a consequence of sintering at 1200 °C, the scaffold structure undergoes crystallisation in parallel with densification (Fig. 3c) and there are consequently significant fractions of wollastonite and pseudo-wollastonite grains within the sintered scaffolds [18,22].

3.2. Scaffold mechanical properties

Compression tests were carried out on samples from all scaffold designs fabricated at both sintering temperatures. There was considerable variation observed for the mechanical response of individual scaffolds taken from each batch of scaffolds fabricated. This can be clearly seen in the montage of stress–strain data obtained from testing several 300scaf structures shown in Fig. 4. However, all of the compression tests show the same features. There is always a region at the begining of each test showing a small increase in stress with increasing compressive strain (up to 0.1% initial apparent strain). This is because the scaffolds are tested in the as-sintered condition and hence their top and bottom surfaces are neither flat nor parallel, thus there is an initial period of specimen rotation within the loading plates of the compression test before each scaffold achieves uniform loading. This is followed by a region of linear elastic deformation before discontinuities occur above a stress of about 10 MPa, these are believed to indicate internal sub-critical fracture of individual struts, before peak load and final crushing occurs at a stress of 15–35 MPa.

It is notable that unlike the behaviour of many brittle foams reported previously, [9] there is no distinctive plateau region of constant crushing strength after peak load, nor there is a regime of increasing stress or densification at large strains. Instead after peak load there is a chaotic regime of decreasing and increasing stress before total collapse of the scaffold and zero resistance to further deformation. This behaviour is similar to that reported by Chopra for similar scaffold designs fabricated from a different glass composition [26] and by Baino and Vitale-Brovarone [28] for a glass–ceramic foam scaffold. A possible reason for this behaviour is the relatively small size of the compression specimens, which contain only 3–5 unit cells across the edge of the specimen. Thus if a single cell strut fails the large amount of stress transfer to the rest of the structure is likely to initiate repeated strut failure and structural collapse. Most of the work reported in the literature on brittle foams has used larger specimens (relative to the unit cell) and thus the failure of individual struts are less likely to lead to total structural failure and a plateau stress is observed. Similar curves, but with the features occuring at different stress levels were seen in all specimens tested. However, the 400scaf and 600scaf structures sintered at 800 °C proved very fragile

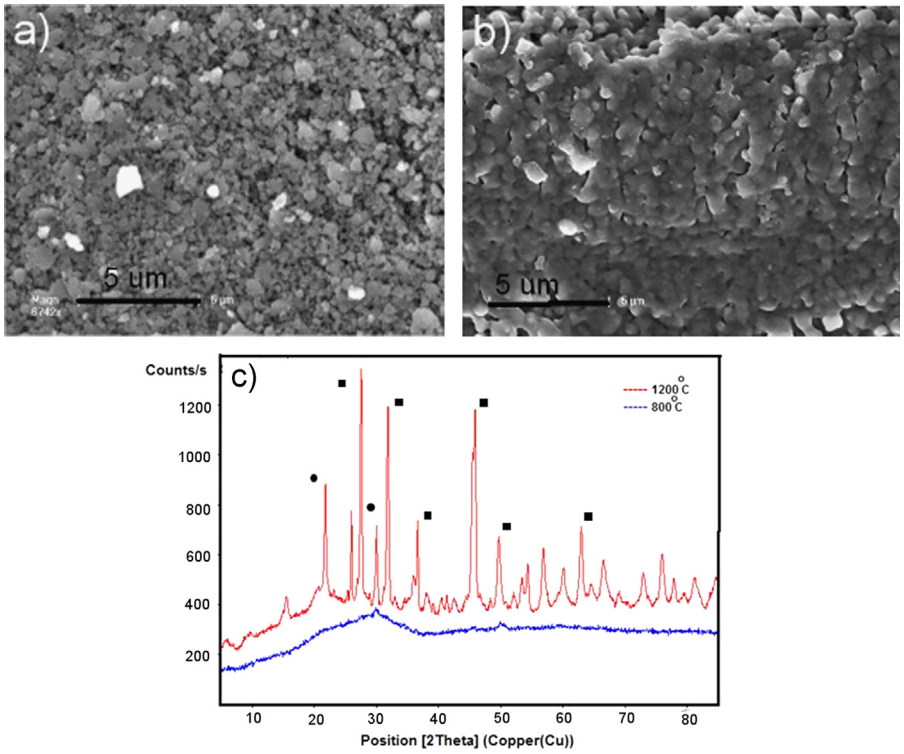

Fig. 3. Comparison of scaffold strut microstructures after sintering (a) sintered at 800 °C, (b) sintered at 1200 °C, (c) XRD traces from struts sintered at 800 and 1200 °C showing the presence of crystal phases, ■ pseudowollastonite, ● wollastonite.

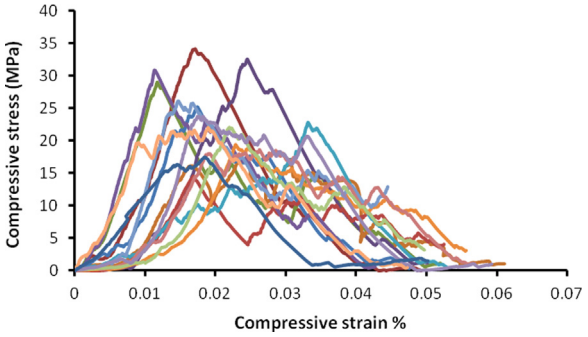

Fig. 4. Montage of a number of stress stain curves obtained from crushing strength experiments on a series of 300scaf sample sintered at 1200 °C.

Table 1
Summary of the mechanical properties for the three scaffold types.

	Pore width (μm)	Strut width (μm)	Elastic modulus (GPa)	Crushing strength (MPa)	Strut strength (MPa)	Number tested	Weibull modulus
Sintered 800 °C							
300scaf	300	370	0.5 ± 0.1	4.7 ± 0.8		15	4.9
Sintered 1200 °C							
300scaf	300	370	2.9 ± 0.6	23.7 ± 5.9	82.5 ± 22.5	15	3.2
400scaf	400	490	1.0 ± 0.1	15.1 ± 4.9	52.6 ± 17.1	15	2.9
600scaf	600	730	0.6 ± 0.1	11.8 ± 4.1	41.1 ± 14.3	15	2.7

and it was not possible to fabricate sufficient samples for mechanical testing. Further discussion on the influence of scaffold architecture will thus be confined to scaffolds sintered at 1200 °C.

The mean peak stress or crushing strength and mean elastic modulus data are reported in Table 1, along with the Weibull modulus, for the scaffolds tested. Assuming that the mechanical properties of the scaffolds are described by the model of Gibson and Ashby for the properties of cellular solids, [9] the strength of a strut in the scaffold is the same as the strength of the bulk material and is related to the strength of the cellular solid (scaffold) by its relative density with

$$\frac{\sigma_{cell}}{\sigma_{bulk}} = 0.65(\rho_R)^{1.5} \quad (1)$$

where ρ_R is the relative density (1 - porosity) of the cellular solid. This computed strut strength is also shown in Table 1.

From Table 1, it is clear that the Weibull modulus values for all scaffolds are low. Conventionally, one would expect Weibull modulus values of solid ceramic specimens to range from 5 to 20 [29,30]. However, other researchers have also found low values of Weibull modulus for ceramic and glass biomaterials. Pirhonen et al. reported Weibull modulus values in the range 2–4 for bioactive glass 9–93 fibres [31]; Baino and Vitale-Brovarone reported a Weibull modulus of 4 for glass ceramic scaffolds produced by sponge replication but they did not report the scaffold porosity [28]. For other brittle foams, the literature values for the Weibull modulus are also low, e.g. in alumina foams the Weibull modulus is reported to be in the range of 1–3, and for reticulated vitreous carbon foams in the range of 4.4–6.2 [9].

3.3. Influence of scaffold dimensions

In order to interpret the mechanical property data for the scaffold structures, we fabricated a number of larger specimens using the same materials and fabrication methods. The intrinsic porosity of the bulk sintered material was measured using the Archimedes method and was determined to be 1.3%. A number of bars, of loaded dimensions 3.5 mm × 4.5 mm × 20 mm, were tested in 4-point bend and a mean failure stress of 6.2 ± 1.3 MPa, with a Weibull modulus $m=4.2$, was determined from a sample of 10 specimens. The hardness and elastic modulus of the bulk material was measured using nanoindentation to give 550 ± 35 MPa and 17.6 ± 2.8 GPa respectively.

The average porosity of the 1200 °C sintered scaffolds was 42%, irrespective of the internal dimensions of the pores and struts. Conventional models of the mechanical properties of porous and cellular materials predict that their strength and elastic modulus, relative to the properties of the corresponding fully dense bulk material, are only functions of the relative density and internal geometry of the material. Thus the observed reduction in both Young's modulus and crushing strength (and hence computed strut strength) with increasing pore size at constant porosity seen in Table 1 is not consistent with simple models for the strength of cellular materials. However, Gibson noted that in brittle materials there is a well known correlation between size and strength, with larger samples of a given ceramic component showing lower values of mean fracture strength, thus larger dimension brittle foams will display lower values of failure stress [9]. This supports previous observations of a decrease in strength with increasing cell dimensions in porous ceramics and glasses [26,32–34]. The Weibull statistics model (weakest link model) for the strength of brittle material states that the mean failure strength of two batches of ceramics tested under the same conditions, σ_1 and σ_2, will scale with their respective tested volumes, V_1 and V_2, by the following relation:

$$\frac{\sigma_1}{\sigma_2} = \left(\frac{V_2}{V_1}\right)^{\frac{1}{m}} \quad (2)$$

where m is the Weibull modulus. Fig. 5 shows the strength of the struts in the scaffold materials (determined using Eq. (1)) plotted against the strut volume. On the same figure we also plot the strength of the bulk specimen tested in bend along with its volume. All four data points are shown to lie close to the linear regression line of gradient −0.29. From Eq. (2) this gradient is equivalent to $-1/m$ or in this case $m=3.4$. Comparing this value with the Weibull modulus data obtained from each of the scaffolds shows that the Weibull modulus is practically the same in all cases.

Gibson and Ashby have derived a simple mechanical model [9] that states that the elastic modulus of a cellular solid is controlled by its relative density and the modulus of the equivalent bulk solid with:

$$\frac{Ecell}{E_{bulk}} = (\rho_R)^2 \quad (3)$$

Using Eq. (3) with a relative density of 0.58 and the bulk Young's modulus of 17.6 GPa, obtained using nanoindentation, the predicted scaffold Young's modulus is 5.9 ± 0.9 GPa, This is significantly greater than the values measured from all scaffolds sintered at 1200 °C (Table 1). A possible reason for this discrepancy could be the rather large displacement that occurs before the sample is accurately located for compression loading (Fig. 5). It is possible that during this stage some damage occurs to the internal struts and this will result in an apparent reduction in the elastic modulus. This mechanism would explain why the experimentally measured Young's modulus is smaller with the larger pore size scaffolds because the larger struts are weaker and thus more susceptible to damage.

Thus we conclude that the variation in scaffold crushing strength with scaffold size is fully explained by the volume dependence predicted using Weibull statistics. The increase in strut strength with decreasing strut dimensions as the scaffold pore size decreases (Table 1) is fully predicted by the strength of larger specimens tested in bend using the volume scaling of Weibull statistics (Eq. (2)) as clearly shown in Fig. 5. From this we can see that the defect distribution introduced during gel casting that leads to a similar statistical strength behaviour at the internal size scale of our scaffolds, with strut dimensions in the range of 400–800 μm, and in larger (mm–cm scale) test pieces.

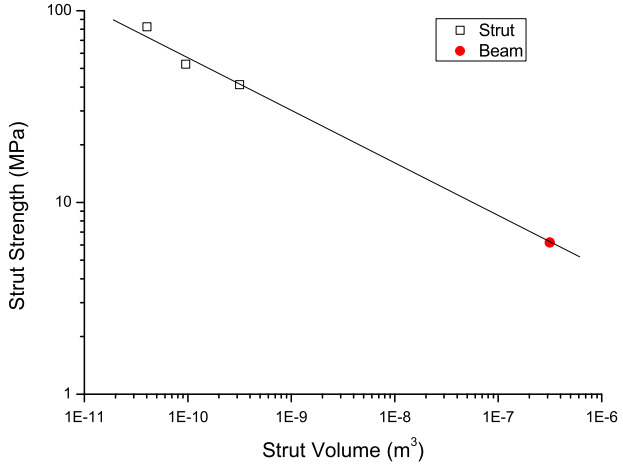

Fig. 5. Computed fracture stress of the struts within the scaffolds plotted against strut volume (square symbols) along with the strength of a bulk specimen tested in 4-point bend (round symbol). Line shows a linear regression to the data, the slope of the line (on a logarithmic scale) is equal to $-1/m$, where m is the Weibull modulus of the fracture data.

4. Conclusions

We have successfully fabricated a range of scaffolds, from slurries of CaO–SiO_2 particles fabricated using a sol–gel route, with internal pore size in the range 300–600 μm using gel casting into moulds fabricated by stereolithography. In order to obtain scaffolds with sufficient mechanical strength to allow easy handling without damage, it was necessary to sinter the structures at a temperature of 1200 °C. At this relatively high

sintering temperature significant crystallisation occurs and the resulting microstructure contains significant fractions of wollastonite and a pseudo-wollastonite phase. All scaffolds were fabricated using a simple cubical symmetry design at a constant porosity of 42%. Scaffolds could be fabricated with pore sizes of 300 μm or larger, smaller scaffolds were difficult to fabricate because of poor penetration of the ceramic slurry into fine moulds.

The mechanical properties of the ceramic scaffolds were found to be strong functions of their dimensions with larger pore size scaffolds showing lower strength and fracture toughness values than the smallest 300 μm pore size scaffold. We have used the simple model for the mechanical properties of cellular materials developed by Gibson and Ashby [9] to interpret our data. Their model for the mechanical properties of brittle foams, coupled with conventional Weibull analysis of ceramic failure strengths, shows fully self consistent behaviour that scales to the mechanical properties of bulk ceramic samples made from the same ceramic powders and processing route. However, the predicted elastic behaviour shows much poorer agreement with Young's modulus of the scaffolds being significantly lower than the values predicted by the Gibson and Ashby model. This needs further investigation but be hypothesise that it may indicate significant internal damage that occurs within the scaffold before the peak crushing strength is reached.

The mechanical properties of the scaffold structures fabricated in this study are similar to the mechanical properties of other ceramic and glass scaffold structures, made from a range of bioactive glasses and ceramics, that have been reported in previous studies in the literature. The statistical variation in our data can be modelled using a Weibull modulus of $m \approx 3$; this is also similar to Weibull modulus values reported for similar porosity ceramic foams. The mean strength of the scaffolds are in the range of 12–24 MPa, which is similar to the lower range of the strength of cortical bone [10] and slightly greater than the strength of cancellous bone [11]. Their elastic properties are closer to those of cancellous bone. However, the range of mechanical properties is sufficiently close to that of hard tissue for these scaffolds to be candidates for use in bone or hard tissue regenerative medicine applications.

Acknowledgements

We would like to thank Julian Jones of Imperial College, London, for the provision of the glass powder used in this study. IS would like to acknowledge the government of Iraq for the provision of a PhD Scholarship. The equipment used in this project was supported by the EPSRC, United Kingdom through Grants EP/L012022/1 and EP/C01328X/1.

References

[1] L.C. Gerhardt, A.R. Boccaccini, Bioactive glass and glass–ceramic scaffolds for bone tissue engineering, Materials 3 (2010) 3867–3910.
[2] D.W. Hutmacher, Scaffolds in tissue engineering bone and cartilage, Biomaterials 21 (2000) 2529–2543.
[3] S.J. Hollister, Porous scaffold design for tissue engineering, Nat. Mater. 4 (2005) 518–524.
[4] C. Liu, Z. Xia, J.T. Czernuszka, Design and development of three-dimensional scaffolds for tissue engineering, Chem. Eng. Res. Des. 85 (2007) 1051–1064.
[5] V. Karageorgiou, D. Kaplan, Porosity of 3D biomaterial scaffolds and osteogenesis, Biomaterials 26 (2005) 5474–5491.
[6] Q.L. Loh, C. Choong, Three-dimensional scaffolds for tissue engineering applications: role of porosity and pore size, Tissue Eng. B 19 (2013) 485–502.
[7] S.M. Lien, L.Y. Ko, T.J. Huang, Effect of pore size on ECM secretion and cell growth in gelatin scaffold for articular cartilage tissue engineering, Acta Biomater. 5 (2009) 670–679.
[8] S.F. Hulbert, F.A. Young, R.S. Mathews, J.J. Klawitter, C.D. Talbert, F.H. Stelling, Potential of ceramic materials as permanently implantable skeletal prostheses, J. Biomed. Mater. Res. 4 (1970) 433–456.
[9] L.J. Gibson, M.F. Ashby, Cellular Solids: Structure and Properties, 2nd edn., Cambridge University Press, Cambridge, UK, 1997.
[10] D.R. Carter, D.M. Spengler, Mechanical-properties and composition of cortical bone, Clin. Orthop. Relat. Res. 135 (1978) 192–217.
[11] L.J. Gibson, The mechanical behaviour of cancellous bone, J. Biomech. 18 (1985) 317–328.
[12] H.R. Ramay, M.Q. Zhang, Preparation of porous hydroxyapatite scaffolds by combination of the gel-casting and polymer sponge methods, Biomaterials 24 (2003) 3293–3302.
[13] A. Almirall, G. Larrecq, J.A. Delgado, S. Martinez, J.A. Planell, M.P. Ginebra, Fabrication of low temperature macroporous hydroxyapatite scaffolds by foaming and hydrolysis of an alpha-TCP paste, Biomaterials 25 (2004) 3671–3680.
[14] J.R. Jones, L.L. Hench, Factors affecting the structure and properties of bioactive foam scaffolds for tissue engineering, J. Biomed. Mater. Res. B 68B (2004) 36–44.
[15] Q.Z. Chen, I.D. Thompson, A.R. Boccaccini, 45S5 Bioglass (R)-derived glass–ceramic scaffolds for bone tissue engineering, Biomaterials 27 (2006) 2414–2425.
[16] B. Derby, Printing and prototyping of tissues and scaffolds, Science 338 (2012) 921–926.
[17] K.F. Leong, C.M. Cheah, C.K. Chua, Solid freeform fabrication of three-dimensional scaffolds for engineering replacement tissues and organs, Biomaterials 24 (2003) 2363–2378.
[18] J.R. Jones, L.M. Ehrenfried, L.L. Hench, Optimising bioactive glass scaffolds for bone tissue engineering, Biomaterials 27 (2006) 964–973.
[19] I.D. Xynos, M.V.J. Hukkanen, J.J. Batten, L.D. Buttery, L.L. Hench, J.M. Polak, Bioglass (R) 45S5 stimulates osteoblast turnover and enhances bone formation in vitro: implications and applications for bone tissue engineering, Calcif. Tissue Int. 67 (2000) 321–329.
[20] L.L. Hench, J.M. Polak, Third-generation biomedical materials, Science 295 (2002) 1014–1017.
[21] N. Patel, S.M. Best, W. Bonfield, I.R. Gibson, K.A. Hing, E. Damien, P.A. Revell, A comparative study on the in vivo behavior of hydroxyapatite and silicon substituted hydroxyapatite granules, J. Mater. Sci. Mater. Med. 13 (2002) 1199–1206.
[22] J.R. Jones, O. Tsigkou, E.E. Coates, M.M. Stevens, J.M. Polak, L.L. Hench, Extracellular matrix formation and mineralization on a phosphate-free porous bioactive glass scaffold using primary human osteoblast (HOB) cells, Biomaterials 28 (2007) 1653–1663.
[23] T.M.G. Chu, J.W. Halloran, S.J. Hollister, S.E. Feinberg, Hydroxyapatite implants with designed internal architecture, J. Mater. Sci. Mater. Med. 12 (2001) 471–478.
[24] O.O. Omatete, M.A. Janney, R.A. Strehlow, Gelcasting - a new ceramic forming process, Am. Ceram. Soc. Bull. 70 (1991) 1641–1649.
[25] M.A. Janney, O.O. Omatete, C.A. Walls, S.D. Nunn, R.J. Ogle, G. Westmoreland, Development of low-toxicity gelcasting systems, J. Am. Ceram. Soc. 81 (1998) 581–591.
[26] K. Chopra, P.M. Mummery, B. Derby, J.E. Gough, Gel-cast glass–ceramic tissue scaffolds of controlled architecture produced via stereolithography of moulds, Biofabrication 4 (2012) 045002.

[27] H. Lu, T. Zhang, X.P. Wang, Q.F. Fang, Electrospun submicron bioactive glass fibers for bone tissue scaffold, J. Mater. Sci. Mater. Med. 20 (2009) 793–798.
[28] F. Baino, C. Vitale-Brovarone, Mechanical properties and reliability of glass–ceramic foam scaffolds for bone repair, Mater. Lett. 118 (2014) 27–30.
[29] R.W. Davidge, Mechanical Behaviour of Ceramics, Cambridge University Press, Cambridge, UK, 1979.
[30] D.J. Green, An Introduction to the Mechanical Behaviour of Ceramics, Cambridge University Press, Cambridge, UK, 1998.
[31] E. Pirhonen, H. Niiranen, T. Niemela, M. Brink, P. Tormala, Manufacturing, mechanical characterization, and in vitro performance of bioactive glass 13–93 fibers, J. Biomed. Mater. Res. B 77B (2006) 227–233.
[32] C.Q. Dam, R. Brezny, D.J. Green, Compressibive behavior and deformation-mode map of an open cell alumina, J. Mater. Res. 5 (1990) 163–171.
[33] J.M. Cordell, M.L. Vogl, A.J.W. Johnson, The influence of micropore size on the mechanical properties of bulk hydroxyapatite and hydroxyapatite scaffolds, J. Mech. Behav. Biomed. Mater. 2 (2009) 560–570.
[34] Q. Fu, E. Saiz, A.P. Tomsia, Bioinspired strong and highly porous glass scaffolds, Adv. Funct. Mater. 21 (2011) 1058–1063.